Available online at www.sciencedirect.com
SCIENCE DIRECT®
Journal of Power Sources 134 (2004) 298–307
JOURNAL OF POWER SOURCES
www.elsevier.com/locate/jpowsour

On the key importance of homogeneity in the electrochemical performance of industrial positive active materials in nickel batteries

M. Casas-Cabanas [a], J.C. Hernández [b], V. Gil [c], M.L. Soria [b], M.R. Palacín [a,*]

[a] *Institut de Ciència de Materials de Barcelona (CSIC), Campus UAB E-08193 Bellaterra, Catalonia, Spain*
[b] *Sociedad Española del Acumulador TUDOR (Exide Technologies), Autovía A-2, km 42 E-19200 Azuqueca de Henares, Guadalajara, Spain*
[c] *Electro Mercantil Industrial S.L. (Exide Technologies), Hierro 38, E-28850 Torrejón de Ardoz, Madrid, Spain*

Received 5 December 2003; received in revised form 8 March 2004; accepted 22 March 2004

Available online 8 June 2004

Abstract

A thorough characterisation of three different commercial positive active materials for nickel batteries was carried out both from the crystal chemical and the electrochemical point of view. All the samples had similar physical characteristics and consisted of mixtures of graphite and β-nickel hydroxide with diverse doping levels. Two different electrode technologies (pasted and pocket plate) were used in all cases. Surprisingly, the best capacity values in pocket plate technology (with no extra conducting additives) were supplied by sample A, that is, the one with the lowest doping level. These good performances were attributed to a higher degree of homogeneity in carbon distribution. This hypothesis was confirmed by milling treatments carried out on sample C that did indeed significantly improve its homogeneity and its electrochemical behaviour. In summary, this work shows that homogeneity is clearly an underestimated factor in industrial active materials. Indeed, instead of more expensive dopant addition, low cost milling processes can be used to obtain commercial active materials with improved capacities.

Keywords: Nickel batteries; Nickel hydroxide

1. Introduction

Despite the emergence of lithium ion technology, nickel based batteries (Ni/Cd, Ni/MH or Ni/H_2) are still widely used for very diverse applications ranging from portable electronics to satellites. Moreover, the Ni/MH technology is currently the most viable battery system for electric and hybrid vehicle applications. Since the first patents by Jungner (Ni/Cd) [1,2] and Edison (Ni/Fe) [3,4], the positive nickel oxyhydroxide electrode (NOE) present in these batteries has been in use for more than a century. Many studies have been devoted to the NOE [5,6], however, the development of its technology has relied often on empirical criteria and the ultimate effect of some additives or dopants (e.g. addition of lithium ions to the electrolyte) is still unknown. Even if the fundamental understanding of the system is not complete, most electrode materials manufacturers have been able to develop procedures for active material preparation that result in good performances of the NOE and hence of the resulting battery. The synthetic procedures include generally the use of an additive (graphite or metallic Ni among others) to enhance the electronic conductivity of the electrodes, that would be low due to the fact that β-Ni$(OH)_2$ is a p-type semiconductor. In addition to this, even if it increases the cost of the active material, cobalt is currently used as a dopant with the objectives of improving charge efficiency [7], achieving higher capacities [8,9], increasing oxygen overpotential [10] or eliminating the presence of a second discharge plateau [11]. Other metals such as cadmium or zinc are sometimes also added as dopants to increase oxygen overpotential and inhibit formation of γ-NiOOH [12,13].

The formulation of the active material is usually dependent on the electrode technology and final battery application. Pocket plate electrodes used in vented batteries for industrial applications include graphite in the active material formulation to increase conductivity and therefore active material efficiency. However, in low maintenance or valve regulated designs (such as cylindrical cells for

* Corresponding author. Tel.: +34-935801853; fax: +34-935805729.
E-mail address: rosa.palacin@icmab.es (M.R. Palacín).

0378-7753/$ – see front matter © 2004 Elsevier B.V. All rights reserved.
doi:10.1016/j.jpowsour.2004.03.050

portable applications) this is achieved by using sintered plate technology, porous nickel substrates or nickel powder as conductivity enhancer.

It is obviously needless to say that the homogeneity of the active material (and hence the distribution of the additives and dopants) is crucial for obtaining the optimum electrochemical performances. In this paper we present a comparative study carried out on three different industrial active materials from diverse origins revealing that the importance of homogeneity can be sometimes underestimated. The samples were thoroughly analysed and characterised from a crystal chemical point of view and their electrochemical yields were tested using two different electrode technologies (pocket plate and pasted). In the first case, the active material was used as-received whereas in the second, extra conductive additives were used. Our results indicate that the electrochemical performances of low cost less doped active material can overcome those of more expensive active materials if they are carefully homogenised. Thus, instead of more complex and more expensive doping, a simple milling process can greatly improve the quality of the final industrial active material.

2. Experimental

Three samples of commercial positive active material for standard pocket plate manufacturing have been studied. They have been labelled A, B and C and all have BET surfaces around 30 m^2/g, contain β-nickel hydroxide as the electroactive material, graphite as a conducting additive and cobalt as a dopant (see physicochemical analysis section and Tables 1 and 2). Sample B also contains zinc as a dopant. The chemical compositions were found to be: $Ni_{1-x}Co_x(OH)_2$ ($x \sim 0.008$) with 15.2% graphite, $Ni_{1-x}Co_xZn_y(OH)_2$ ($x \sim 0.025$, $y \sim 0.003$) with 16.7% graphite and $Ni_{1-x}Co_x(OH)_2$ ($x \sim 0.015$) with 13.9% graphite, for samples A, B and C, respectively. A sample of the graphite (mixture of 20% powder and 80% flakes both supplied by Graphitwerk Kropfmühl AG with carbon content >99.5%) used as conducting additive in C was also available and its XRD pattern was measured with comparative purposes.

X-ray diffraction (XRD) patterns were collected using a Rigaku Rotaflex Ru 200-B with Cu Kα ($\lambda = 1.5406$ nm) radiation in the range $2\theta = 5$–90° at a scanning rate of 4°/min. An optical microscope Nikon Optiplot-M was used to study additive distribution and homogeneity of the samples whereas a scanning electron microscope (SEM) JEOL JSM-6300 with a resolution of about 3.5 nm was used to study the morphology of the particles and to investigate if degradation had occurred on pasted electrodes after cycling. Specific surface areas were measured with a Micromeritics Flow Sorb II 2300 system according to the Brunauer–Emmet–Teller (BET) multipoint method by nitrogen physisorption at 77 K. Samples were previously dried under vacuum for 14 h, and the free space was measured with helium gas at 77 K.

Table 2
Results of chemical analysis for samples A, B and C. β weight percent refers to β-$Ni_{1-x}Co_x(OH)_2$ content

Sample	% Ni	% Co	% Zn	% SO_4^{2-}	% C	% β
A	47.1	0.41	0	0.2	15.28	78.13
B	49.4	1.26	0.17	1.4	19.68	76.19
C	49.2	0.75	0	1.2	13.96	79.06

Granulometry of the samples was measured with a multi-sieve system EML 200 (Haver & Boecker) with sieves in the range 10–150 μm, whereas apparent density was determined using a volume known pycnometer.

IR spectra were recorded using a Perkin Elmer Spectrum One FTIR spectrophotometer and were performed on pellets made by mixing a small amount of sample with KBr, that had been previously dried at 125 °C. For TGA studies, a Perkin Elmer TGA 7 thermobalance was used and analyses were made with ca. 40 mg of sample placed in an alumina crucible that were heated at 1 °C/min up to 500 °C. About 0.5 g of sample were dissolved in diluted hydrochloric acid and filtered for chemical analysis. The cobalt content was determined by atomic absorption using a Varian 300 Plus spectrophotometer. For nickel content determination, 35% ammonia was added to this solution that turned blue due to the formation of nickel and cobalt hexaamino complexes and electrodeposition of both nickel and cobalt was carried out on a Winkler platinum electrode at 18 mA/cm^2 up to disappearance of the blue colour. Graphite and sulphate contents were determined gravimetrically after dissolution of ca. 3 g of sample by weighing the insoluble residue in the first case and by adding barium chloride to induce the precipitation of barium sulphate in the second.

2.1. Electrode preparation

Pasted electrodes were prepared as follows: 67.5% of the commercial positive active material either A, B or C, 30% of nickel powder (INCO 210, BET surface: 1.5–2.5 m^2/g, apparent density: 0.80 g/cm^3) used as an electronic conductor and 2.5% of polytetrafluoroethylene (PTFE, Aldrich,

Table 1
Values of granulometry, BET surface and apparent density measurements for samples A, B and C

Sample	150 μm (%)	75 μm (%)	25 μm (%)	15 μm (%)	<10 μm (%)	BET surface (m^2/g)	Apparent density (g/cm^3)
A	44.8	22.9	23.7	7.2	1.4	29.2	1.52
B	54.1	22.8	15.6	6.6	0.9	34.7	1.55
C	59.4	18.9	18.5	2.6	0.6	33.6	1.52

60% weight dispersion in water, viscosity ca. 20 cps) used as a mechanical binder were mixed to form the active paste. A nickel foam support (Goodfellow, 96.5% porosity, 43 pores/cm, thickness: 1.6 mm thick) was impregnated with the paste. These electrodes were dried at 50 °C, cut into disks (0.79 cm^2) and pressed at about 2 t/cm^2.

Pocket plate electrodes were prepared by placing 50 mg of commercial positive active material into a nickel grid. The grid was folded into a disk (0.79 cm^2) and this resulting electrode was pressed at about 0.25 t/cm^2.

The electrochemical tests were carried out using a 8-channel Arbin BT2402 cycling system operating in galvanostatic mode. Teflon Swagelok laboratory test cells were used. Positive and negative electrodes were separated by a polypropylene separator (SCIMAT) impregnated with a 5 M KOH solution. All the potentials given in this paper have been recorded versus $Cd/Cd(OH)_2$ pasted type electrodes prepared with commercial negative active material consisting of cadmium oxide with ca. 6% iron oxide and 7% graphite added.

3. Results and discussion

3.1. Physicochemical analysis

The results of granulometry, BET surface and apparent density measurements of the three industrial samples are indicated in Table 1, whereas those of the chemical analysis are shown in Table 2. The physical characteristics of the three samples are very similar, as could be expected from the fact that all of them correspond to optimised industrial materials.

However, important differences exist in the chemical composition. With respect to the conductive additives, they were found to contain only graphite in rather similar amounts, sample B having about 5% more graphite than samples A and C. Concerning to dopants, sample A presents much lower doping level, as it contains only 0.4% Co, whereas sample C contains ca. 0.9% Co and sample B is the one with higher doping level as it contains ca. 1.3% Co in addition to ca. 0.2% Zn. The results allow to calculate the weight percent of β-phase in the sample, that ranges from 76% in sample B to 78–79% in samples A and C. In addition, the three samples were found to contain some sulphate ions, presumably a residue from the synthesis. This makes us suppose that the synthesis was, in the three cases, a direct precipitation reaction derived from the addition of an alkaline solution (e.g. NaOH) to $NiSO_4$ [14]. Infra-red spectra of the samples were indeed consistent with the presence of adsorbed sulphate ions for the three samples.

3.2. Crystal chemical characterisation

X-ray diffraction of the samples (see Fig. 1) shows the unambiguous presence of β-nickel hydroxide in addition

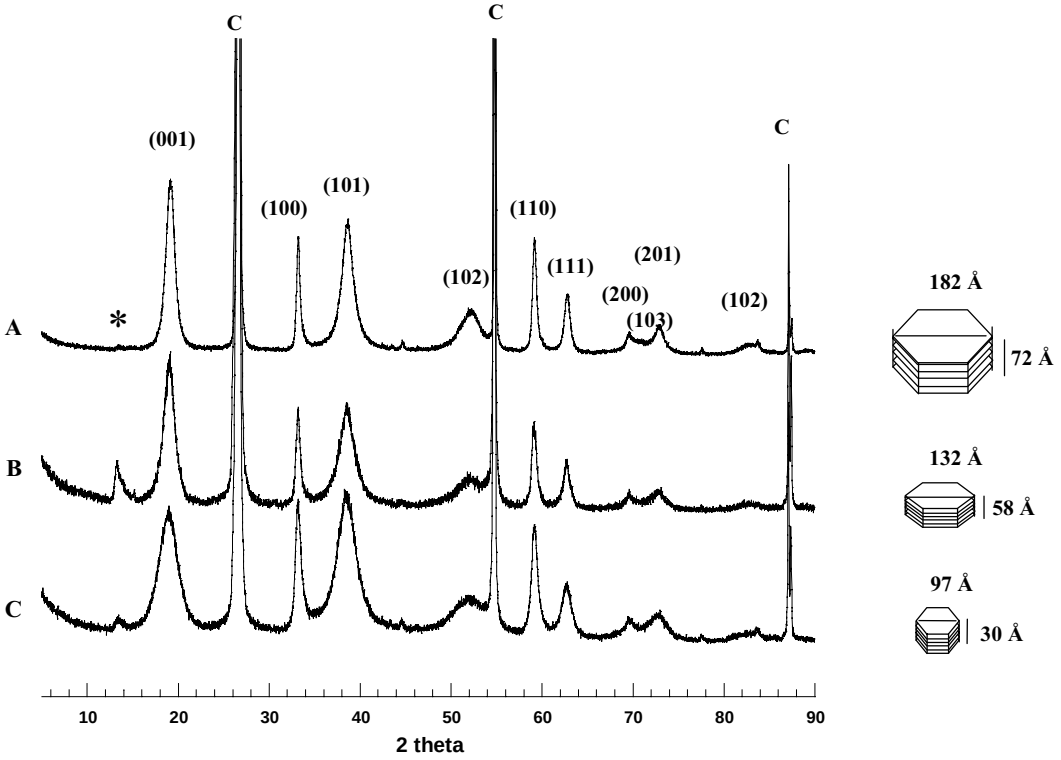

Fig. 1. XRD patterns of samples A, B and C and scheme of the corresponding hexagonal crystallites whose size has been calculated using the Scherrer formula. The asterisk denote an impurity coming from the graphite used as additive.

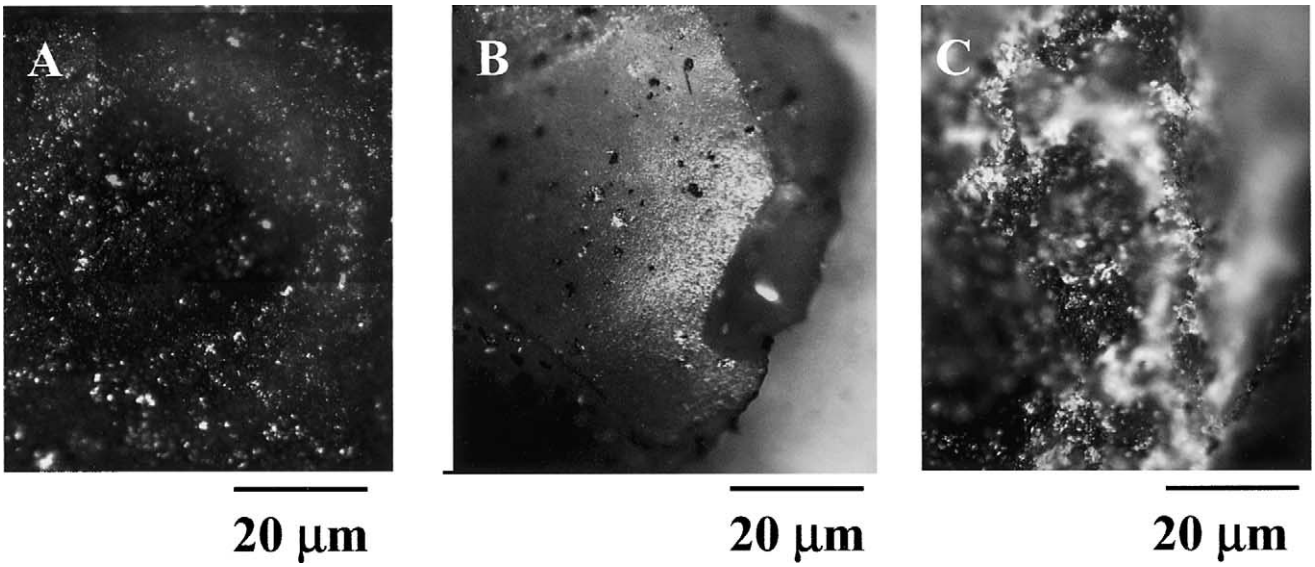

Fig. 2. Images of samples A, B and C obtained by optical microscopy.

to very intense reflections corresponding to graphite, and a peak at around 14° due to an impurity that was also present in the X-ray diffraction pattern of the pristine graphite used as additive in sample C. No traces of α-nickel hydroxide could be detected. The absence of α was confirmed by IR and TGA measurements, as the samples exhibit only a two-step transformation corresponding to the loss of adsorbed water molecules around 60 °C and dehydroxylation of the hydroxide layers at about 250 °C. No traces of the loss of intercalated water molecules around 100 °C typical of the α-phase [15] were observed for any of the samples.

X-ray diffraction patterns allowed also the calculation of the crystallite size by means of the Scherrer formula. The dimensions obtained in the [0 0 1] and [1 0 0] directions are also indicated in Fig. 1. As can be seen, samples A and B present rather similar sizes (slightly larger for A) whereas the values obtained for sample C are about 50% smaller in both directions. The cell parameter was refined and found to be 4.66(3) Å in the three cases.

By optical microscopy performed on the three samples (Fig. 2) we were able to observe that they are formed by agglomerates, containing green nickel hydroxide and black graphite, that present a wide size distribution that ranges from 10 to 250 μm in samples A and C and to 620 μm in sample B. This fact indicates that though the results of granulometry indicated in Table 1 were similar for the three samples, the agglomerates retained in the 150 μm sieve were larger for sample B than for samples A and C. In addition to the size, the aggregates show important differences in colour that indicate strong differences in the distribution of graphite.

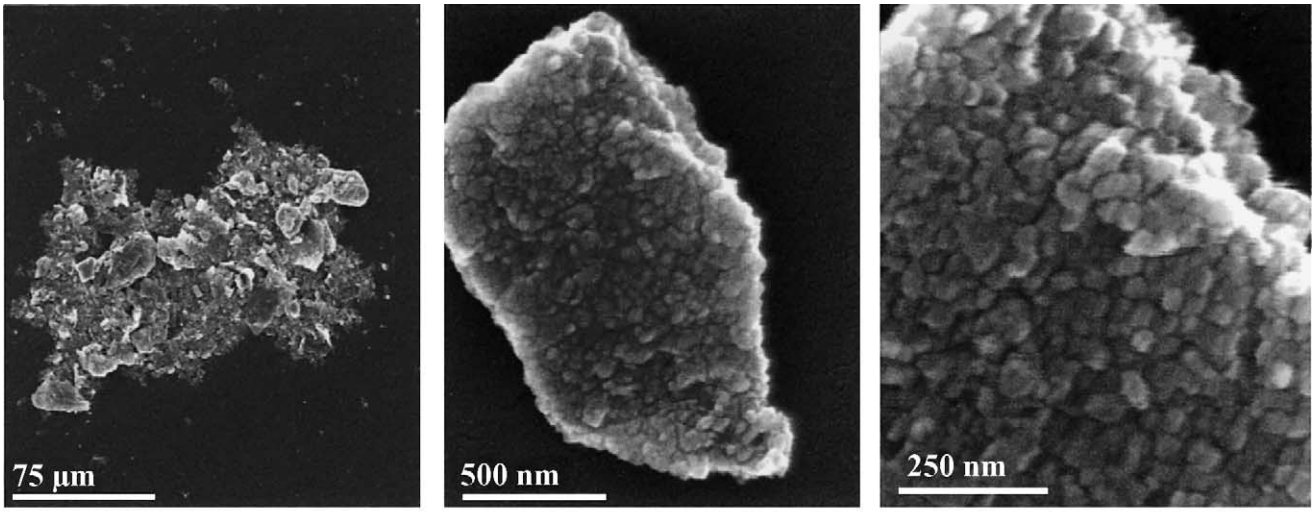

Fig. 3. SEM images of sample A, each one corresponding to an enlargement of the former: (a) macro-agglomerates, (b) meso-agglomerates, and (c) nanometric crystallites.

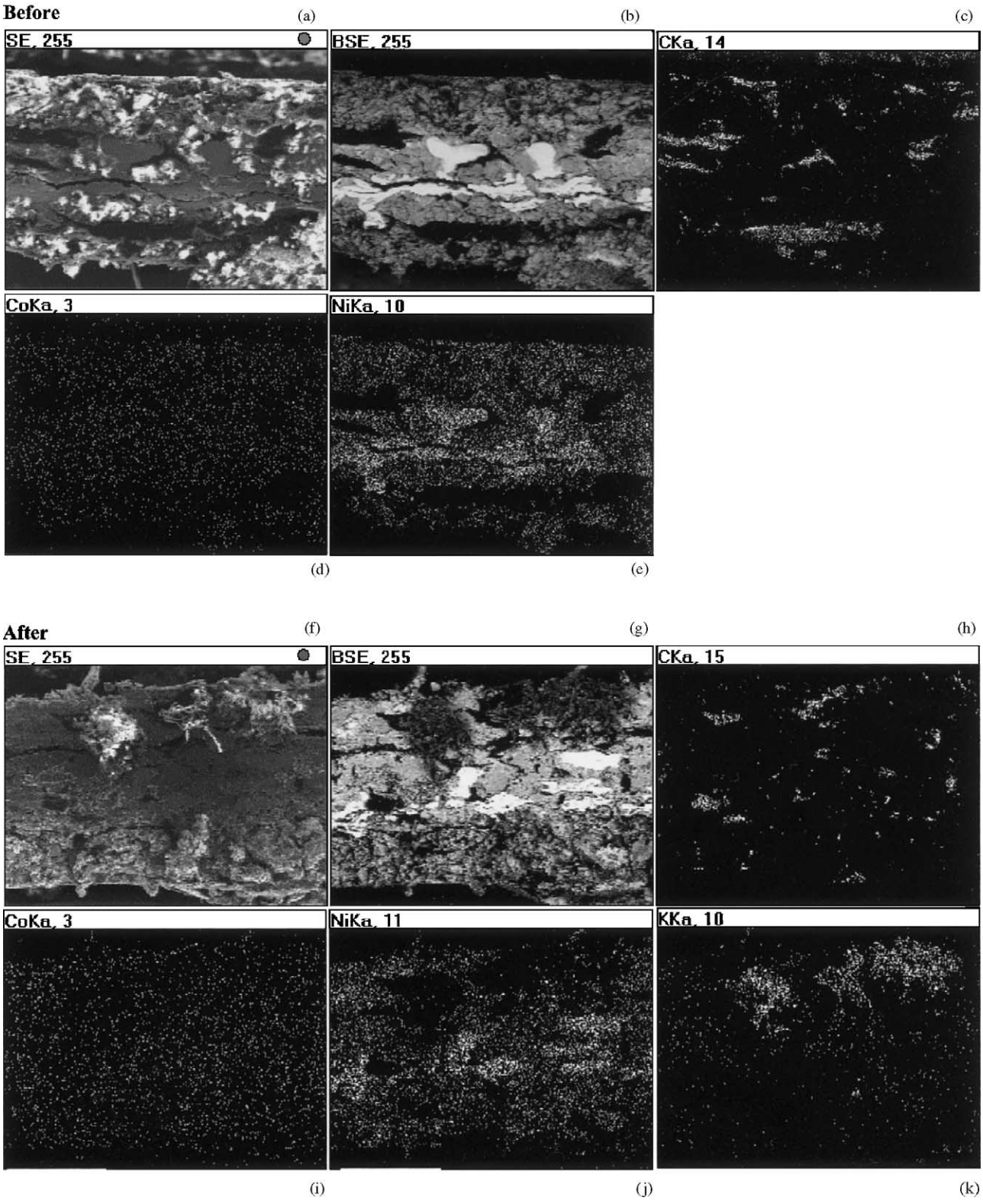

Fig. 4. (a)–(e) SEM images of a pasted electrode section of sample C before cycling: (a) secondary electrons, (b) backscattered electrons, (c) carbon EDX mapping, (d) cobalt EDX mapping, (e) nickel EDX mapping. (f)–(k) SEM images of a pasted electrode section of sample C after cycling: (f) secondary electrons, (g) backscattered electrons, (h) carbon EDX mapping, (i) cobalt EDX mapping, (j) nickel EDX mapping, (k) potassium EDX mapping.

Table 3
Capacity values at cycles 8 and 13 at $C/5$ and at $1.7C$ during the rate capability tests for both pasted and pocket plate electrodes with its standard deviation in brackets

Sample	C_{pasted}, cycle 8 ($C/5$)	C_{pasted}, cycle 13 ($C/5$)	C_{pocket}, cycle 8 ($C/5$)	C_{pocket}, cycle 13 ($C/5$)	C_{pasted} ($1.7C$)	C_{pocket} ($1.7C$)
A	197 (4)	197 (3)	174 (11)	175 (12)	181 (3)	135 (7)
B	232 (1)	230 (1)	139 (32)	134 (35)	179 (11)	72 (19)
C	218 (4)	220 (1)	151 (12)	143 (14)	200 (4)	74 (8)

It is difficult to distinguish between nickel hydroxide and graphite in the aggregates of sample A, whereas for sample C small green zones are clearly distinguishable. In the case of sample B, the aggregates show very large green areas, indicative of poor homogeneity in the distribution of graphite.

The scanning electron microscopy experiments allow the observation of three levels of organisation (see images from sample A as an example in Fig. 3). The agglomerates observed in the optical microscope (Fig. 3(a)) are composed of smaller particles (Fig. 3(b)) whose diameter ranges from

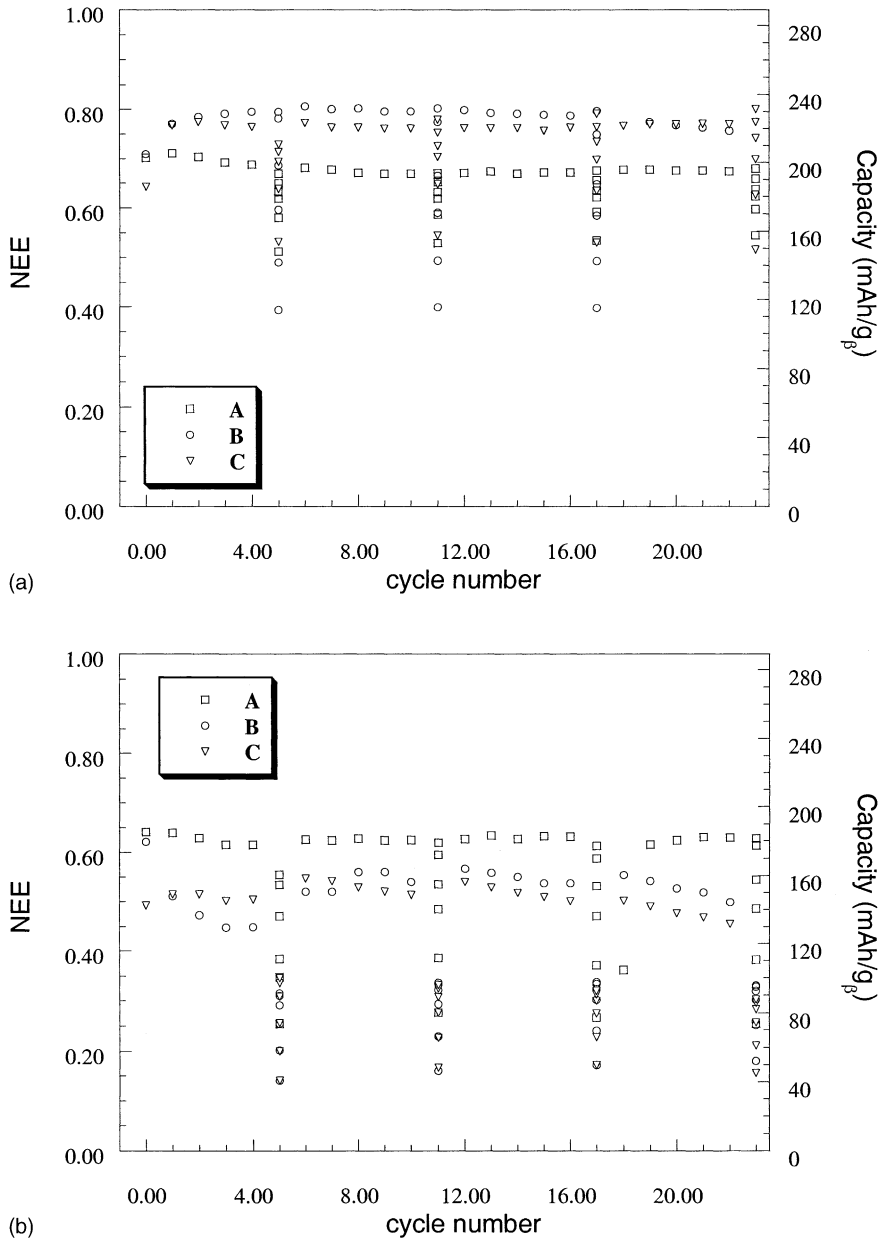

Fig. 5. Plot of capacity (expressed in terms of NEE, number of exchanged electrons per mole of β-$Ni_{1-x}Co_x(OH)_2$, as well as in mAh/g) vs. cycle number for (a) pasted electrodes and (b) pocket plate electrodes.

0.1 to 25 μm in samples A and C and to 30 μm in B. These particles are still an agglomeration of nanometric crystallites (Fig. 3(c)), that present sizes comparable to those calculated from the Scherrer formula [16].

3.3. Electrochemical tests

Electrochemical tests were carried out for the three samples using both pocket plate and pasted electrode technology. The electrodes were cycled at C/5 (e.g. 2.89 mA for an electrode containing 50 mg of β-$Ni_{1-x}Co_x(OH)_2$) with 50% overcharge and discharged down to 1 V versus $Cd/Cd(OH)_2$, with rate capability tests intercalated every five cycles. These consisted of successive discharges at 5*C*, 3.3*C*, 1.7*C*, *C*/1.2, *C*/3 and a final discharge at *C*/6, all of them down to 0.8 V versus $Cd/Cd(OH)_2$. The electrodes were examined by XRD and SEM after cycling. XRD results indicate a small loss of crystallinity upon cycling as expected, but no major modifications are observed.

SEM investigations on pasted electrodes (Fig. 4) before and after cycling indicate a good stability of the electrode: (b) corresponds to a compositional image obtained from backscattered electrons (BSE) where lighter elements appear darker in contrast to heavier elements. This image, together with EDX mapping (c)–(e), clearly allowed to distinguish the nickel foam support in the centre of the electrode section and the pasted positive active material. Graphite distribution throughout the electrode is relatively uniform and cobalt is homogeneously distributed all over the paste. The images obtained after cycling show a good state of the electrode with no signs of degradation or detachment of active material. The only difference is the presence of KOH electrolyte residues crystallised on the electrode's surface. Again, BSE (g) and EDX (h)–(k) images indicate a homogeneous distribution of additives and dopants that does not seem to be altered upon cycling.

The overall electrochemical results were, as expected, very dependent on electrode technology. Table 3 shows some indicative capacity values at cycles 8 and 13 for both pasted and pocket plate electrodes. The fact that both values are similar in all cases indicates that rate capability tests do not cause any degradation of the electrodes whereas standard

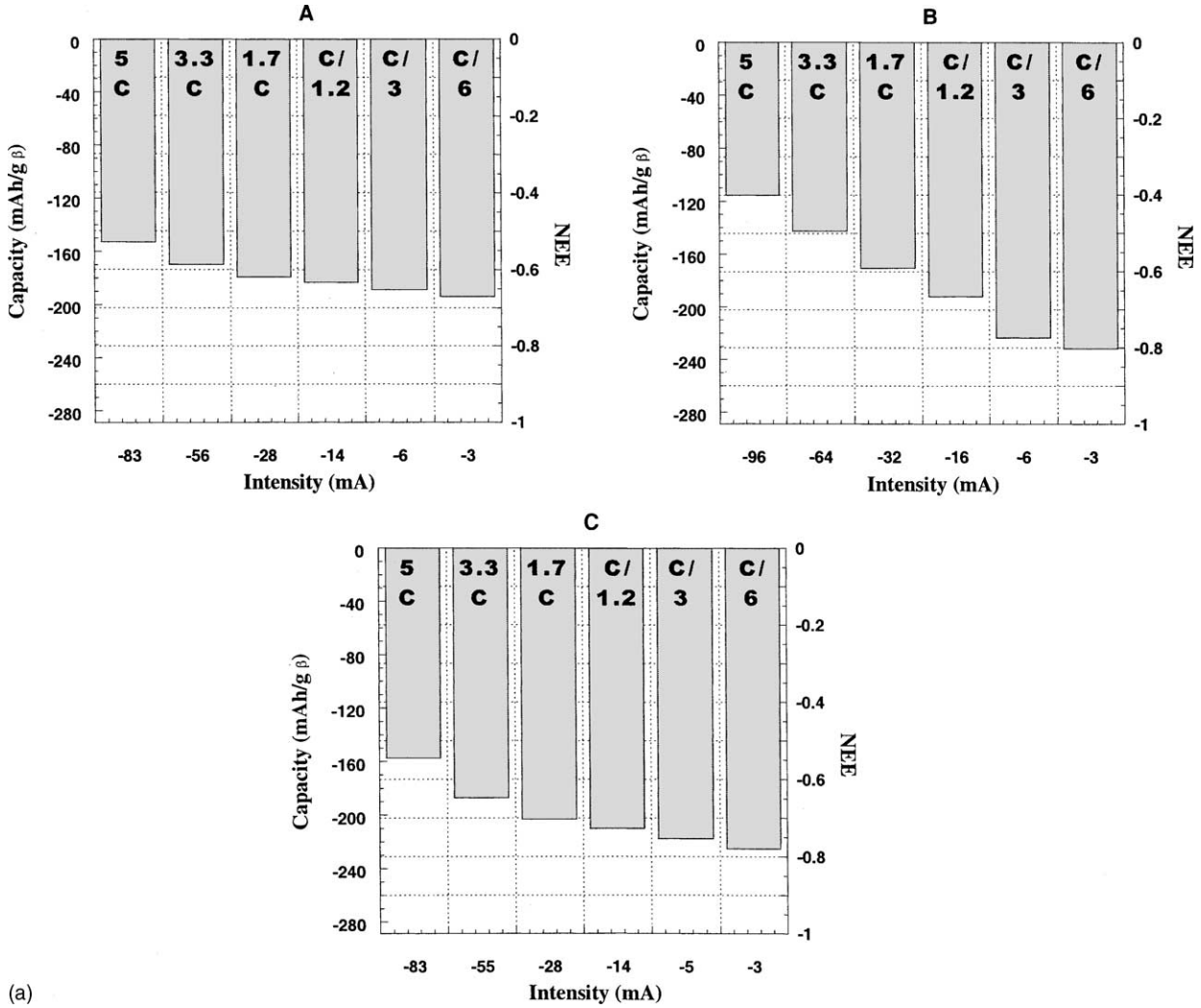

Fig. 6. Rate capability tests for samples A, B and C using: (a) pasted electrodes and (b) pocket plate electrodes.

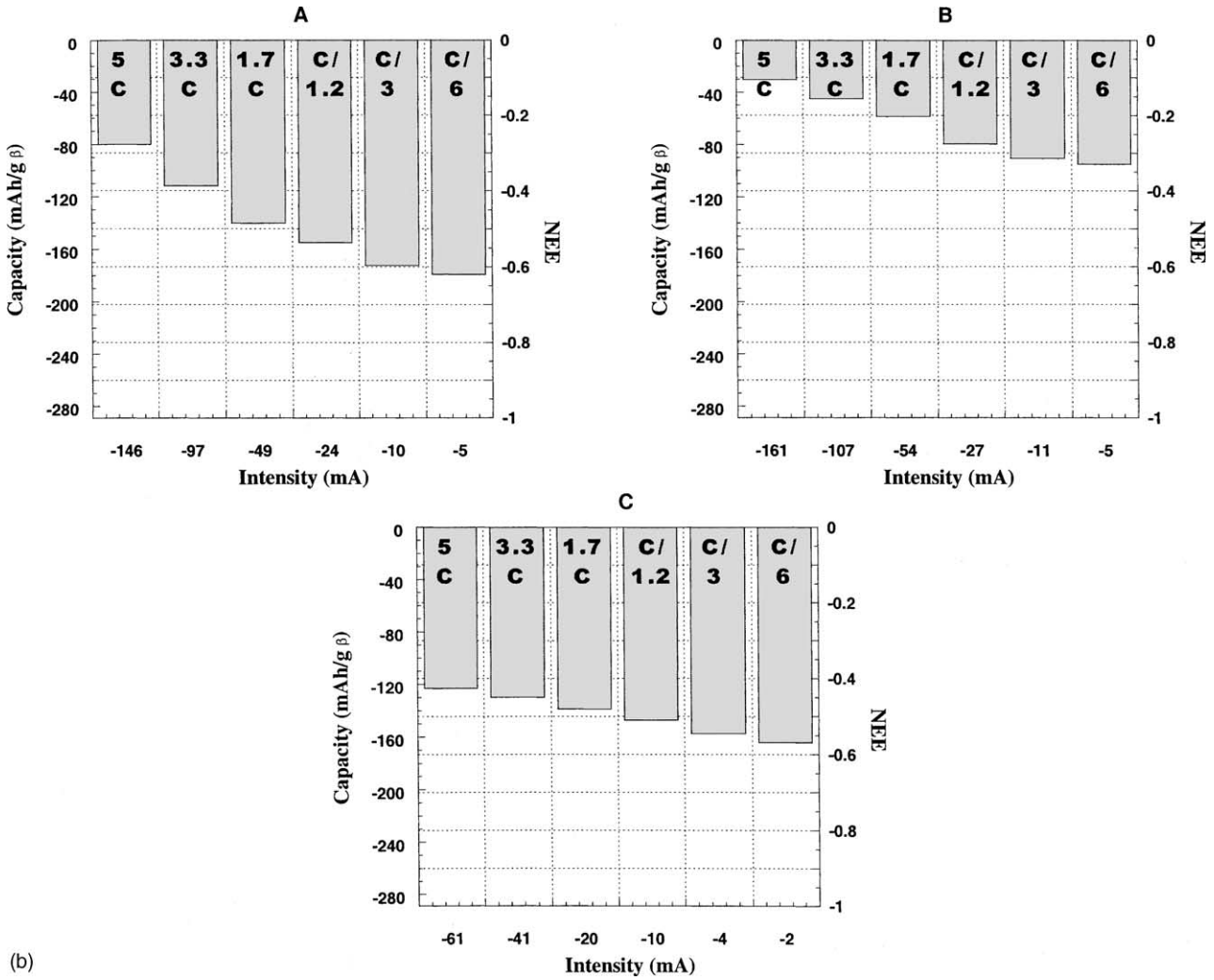

Fig. 6. (*Continued*).

deviation gives an idea of the reproducibility of the experiments. The results obtained for pasted electrodes were found to be, as expected, much more reproducible. The capacity obtained at 1.7*C* during the rate capability tests is also included in Table 3 for comparative purposes.

In the case of pasted electrodes, the plot of capacity (expressed in terms of NEE, number of exchanged electrons per mole of β-$Ni_{1-x}Co_x(OH)_2$, as well as in mAh/g) versus cycle number and a bar diagram including the rate capability results are shown in Figs. 5(a) and 6(a). Upon cycling at *C*/5, B and C samples yield similar capacity values, around 230 mAh/g for the former and 220 mAh/g for the latter. These are a bit higher than the value obtained for sample A (200 mAh/g), a result that can be explained by the lower doping level of this sample. The similarity of results for samples B and C is somewhat unexpected, as the former contains a higher amount of cobalt in addition to zinc. The rate capability tests yield also worse results than expected for sample B. Indeed, it is the one presenting higher doping level but the capacity decreases quickly when increasing the discharge rate. On the other hand, sample A presents remarkably good performances and even at very high rates, the results are similar to those obtained for sample C.

The results of the tests using pocket plate electrodes are shown in Figs. 5(b) and 6(b). With this electrode technology sample A is clearly the one showing the highest capacity values reaching 175 mAh/g in comparison to 140–150 mAh/g for samples B and C. In addition to yielding lower capacity values, electrodes prepared with sample B are also those presenting lower reproducibility. The rate capability tests indicate that sample A presents very good performances and only at high rates sample C presents better yields. As for the case of pasted electrodes, sample B presents very low capacities independently of the working rate. In fact, the capacity values for pocket plate electrodes (with no added nickel powder) prepared with sample A are surprisingly close to those obtained for pasted electrodes, whereas for samples B and C lower yields are always obtained with pocket plate electrodes.

It is obvious that the results of these electrochemical tests and the best performances of sample A cannot be explained in terms of doping level, because it is lower in this sample. The fact that pocket plate electrodes prepared with sample A, with no added conductors, present results similar to pasted electrodes, for which the conductivity is optimised, suggests that conductivity cannot be improved for this sample. As this is not related to the content of conducting additive, that is also lower for sample A than for sample C, and similar to that of sample B, it can only be due to its distribution. Indeed, microscopy studies indicated a very homogeneous distribution of graphite and nickel hydroxide for sample A. Thus, even containing only 0.4% of Co doping and about 15% graphite, the electrodes prepared with sample A outperform the yields of those prepared with sample C containing 0.75% of Co and 14% graphite. The worse results are obtained for sample B despite containing 1.2% Co, 0.17% Zn and 19% graphite and this fact can be once again correlated to the lower homogeneity of this sample, as determined by optical microscopy.

3.4. Effect of additional milling treatment

The improvement of the electrochemical performances with a simple milling treatment was tested on sample C, that was milled on a low energy jar rolling mill for 1, 5, 10 h, 1 day and 3 days at 250 rpm. XRD of the samples after milling do not show any significant change (see Fig. 7) whereas even with a naked eye it is possible to observe a slight gradation in colour that reaches the darkest tones for the samples milled for a longer time showing evidence of a more homogeneous graphite distribution.

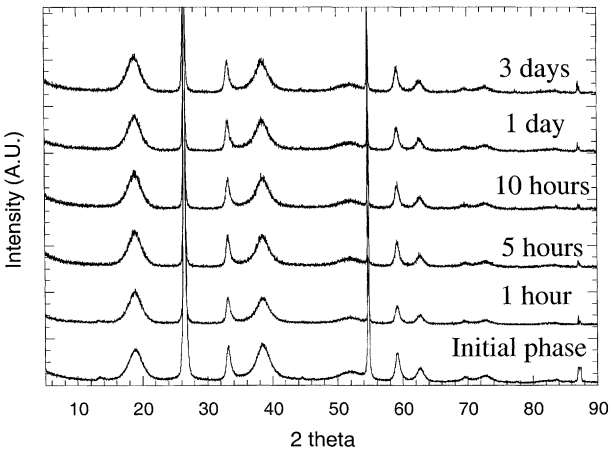

Fig. 7. XRD patterns of sample C before milling and after 1, 5, 10 h, 1 day and 3 days milling treatment.

The electrochemical tests on milled samples were only conducted with pocket plate electrodes to avoid the presence of extra conducting additives. The plot of capacity versus cycle number is shown in Fig. 8 and the increase in capacity upon milling time can be clearly seen. The optimum milling time seems to be around 24 h but we believe that, from the industrial point of view, the duration of the treatment could be significantly reduced if a higher energy mill was used. Increasing milling time above 24 h did not result in improved properties, thus indicating that optimum homogeneity was reached. The capacity of sample C milled for 24 h clearly overcomes that of sample A after the first 4–5 formation cycles, as could be expected from its slightly higher doping

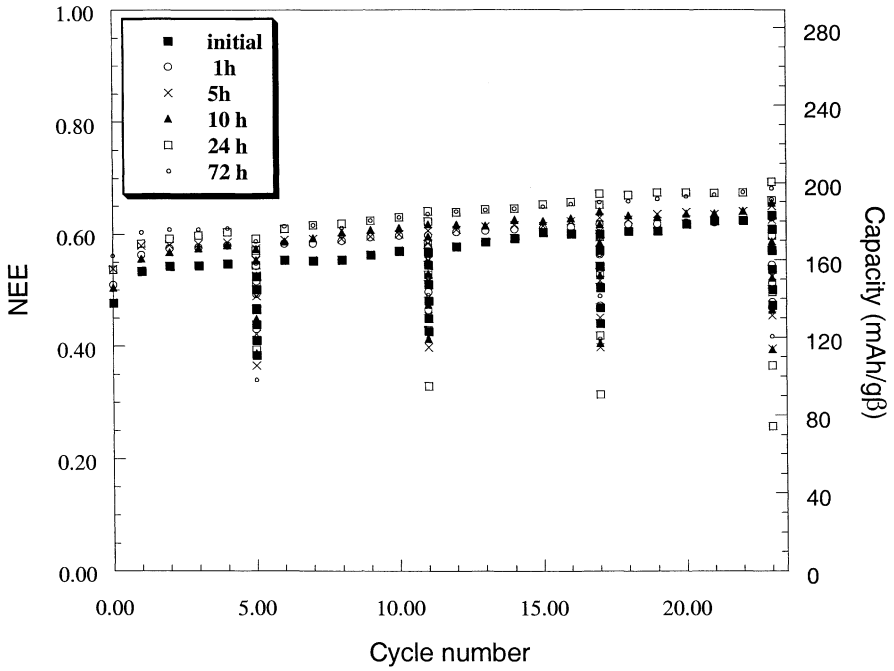

Fig. 8. Plot of capacity (expressed in terms of NEE, number of exchanged electrons per mole of β-$Ni_{1-x}Co_x(OH)_2$, as well as in mAh/g) vs. cycle number for sample C before milling and after 1, 5, 10 h, 1 day and 3 days milling, using pocket plate electrodes.

level, this fact being a clear proof that the very good electrochemical efficiency of sample A is correlated to its higher homogeneity.

4. Conclusions

The three industrial positive active materials studied were similar from a physical point of view, all consisting of mixtures of graphite and β-nickel hydroxide with diverse doping levels. The fact that sample A presented better electrochemical capacities in pocket plate electrodes, being the less doped but also the most homogeneous one, suggested that the good performances were due to a high degree of homogeneity in carbon distribution. This hypothesis was confirmed by milling treatments carried out on sample C that did indeed significantly improve its homogeneity and its electrochemical behaviour as expected. These results indicate that low cost homogenising steps, such as milling, can bring about greater improvements of the active material performances than the more expensive addition of dopants, and hence are of relevant practical interest for battery electrode materials manufacturers.

Acknowledgements

We are grateful to Dr. Joaquín Chacón (Electro Mercantil Industrial S.L.) for helpful discussions and we thank the CSIC for a pre-doctoral fellowship awarded to Montse Casas and the Ministerio de Ciencia y Tecnología for financial support (MAT2000-0128-P4-03).

References

[1] W. Jungner, Swedish Patent 15,567 (1901).
[2] W. Jungner, German Patent 163,170 (1901).
[3] T.A. Edison, German Patent 157,290 (1901).
[4] T.A. Edison, US Patent 678,722 (1901).
[5] P. Oliva, J. Leonardi, J.F. Laurent, C. Delmas, J.J. Braconnier, M. Figlarz, F. Fievet, A. de Guibert, J. Power Sour. 8 (1982) 229–255.
[6] J. McBreen, Modern Aspects of Electrochemistry, vol. 21, Plenum Press, New York, 1990, pp. 29–63.
[7] M. Oshitani, M. Yamane, S. Hattori, Power Sour. 8 (1981) 471–488.
[8] W. Lee, J. Electrochem. Soc. 132 (1985) 2835–2838.
[9] A. Audemer, A. Delahaye, R. Fahri, N. Sac-Epée, J.M. Tarascon, J. Electrochem. Soc. 144 (1997) 2614–2620.
[10] R.D. Armstrong, G.W.D. Briggs, J. Appl. Electrochem. 18 (1988) 215–219.
[11] B. Klapste, K. Micka, J. Mrha, J. Vondrak, J. Power Sour. 8 (1982) 351–357.
[12] M. Oshitani, T. Takayama, K. Takashima, S. Tsuji, J. Appl. Electrochem. 16 (1986) 403–412.
[13] M.E. Uñates, M.E. Folquer, J.R. Vilche, A.J. Arvia, Electrochem. Soc. Proc. 90 (4) (1990) 134–162.
[14] S.U. Falk, A.J. Salkind, Alkaline Storage Batteries, Wiley, New York, 1969, pp. 54–56.
[15] A. Delahaye-Vidal, K. Tekaia Ehlsissen, P. Genin, M. Figlarz, Eur. J. Solid State Inorg. Chem. 31 (1994) 823–832.
[16] Z.S. Wronski, G.J.C. Carpenter, D. Martineau, P.J. Kalal, Electrochem. Soc. Proc. 97 (18) (1997) 804–811.